Small-Signal Stability of HVDC-Connected Offshore Wind Farms Under Weak-Grid Conditions

ANDILE S. XABA[1,2], RUDIREN SARMA[3], DAVID G. DORRELL[4]
[1]School of Engineering, University of KwaZulu-Natal,
Durban,
SOUTH AFRICA

[2]Eskom Holdings SOC Limited,
SOUTH AFRICA

[3]School of Engineering, University of KwaZulu-Natal, Durban,
SOUTH AFRICA

[4]University of Turku, Turku,
FINLAND

Abstract: This paper investigates the small-signal stability of an offshore wind farm connected to a weak onshore AC network through voltage-source-converter-based high-voltage direct-current transmission. An eight-state reduced-order model represents the offshore grid-forming converter, onshore phase-locked loop (PLL), active-power control, DC-link voltage regulation, and battery energy storage system (BESS). Eigenvalue analysis is used to assess the effects of short-circuit ratio (SCR), PLL natural-frequency scaling, wind-power loading, and BESS inclusion. Reducing the SCR from 10 to 1 decreases the damping ratio of the PLL-related mode from 0.571 to 0.285. Increasing the PLL scaling factor from 0.5 to 2.0 raises the modal frequency from 7.41 Hz to 29.51 Hz while maintaining an approximately constant damping ratio. Wind-loading effects are comparatively small, and BESS inclusion provides supplementary reactive-power and voltage support without materially changing the principal PLL-related mode.

Key-Words: Battery energy storage system, eigenvalue analysis, grid-following converter, HVDC transmission, offshore wind integration, phase-locked loop, small-signal stability, weak grid.

Received: April 17, 2026. Revised: June 16, 2026. Accepted: July 28, 2026. Published: November 10, 2026.

1 Introduction

The continued growth of offshore wind generation has increased the use of voltage-source-converter-based high-voltage direct-current (VSC-HVDC) transmission for connecting remote offshore generation to onshore power systems. VSC-HVDC technology enables controllable long-distance power transfer, independent regulation of active and reactive power, and electrical decoupling between offshore and onshore AC networks. These characteristics make it particularly suitable for large offshore wind farms and converter-dominated power systems [1], [2].

However, increasing dependence on power-electronic converters introduces stability phenomena that differ from those traditionally associated with synchronous-machine-dominated systems. Converter control loops operate over multiple time scales and may interact with network impedance, DC-link dynamics, and other converter controllers. These interactions can produce oscillatory or weakly damped modes that are not adequately characterised by conventional steady-state performance criteria alone [3], [4], [5].

A particularly important challenge occurs when an HVDC-connected offshore wind farm is integrated with a weak onshore AC network. Weak-grid conditions are commonly characterised by a low short-circuit ratio (SCR), corresponding to a comparatively high equivalent network impedance relative to the converter rating. Under these conditions, converter-current perturbations produce larger changes in the voltage at the point of common coupling (PCC), thereby strengthening the interaction between converter controls and the surrounding network [6], [7].

The onshore grid-following VSC uses a phase-locked loop (PLL) to estimate the grid-voltage angle and establish the synchronous reference frame required by its control system. A perturbation in converter current affects the PCC voltage through the network impedance, while the resulting voltage-angle perturbation is measured by the PLL and fed back through the converter control system. The resulting feedback path links the PLL dynamics to the strength and impedance characteristics of the onshore AC network [8], [9].

Previous studies have shown that PLL

behaviour and grid strength are closely related in weak-grid converter applications. Increasing the PLL bandwidth improves phase-tracking speed and changes the frequency of the associated synchronisation mode. More detailed converter models may also exhibit reduced PLL-mode damping as the bandwidth is increased under weak-grid conditions [9], [10], [11]. The extent of this behaviour depends on the converter-control structure, network impedance, operating point, measurement filtering, and retained model states.

Small-signal stability analysis provides a systematic framework for investigating these interactions. By linearising the system around a steady-state operating point, the dominant dynamics can be represented using a state-space model. The eigenvalues of the resulting state matrix indicate modal decay, oscillation frequency, damping ratio, and proximity to the small-signal stability boundary. State participation factors can additionally be used to relate individual modes to the physical and control states represented in the model.

Reduced-order modelling is particularly useful when the objective is to identify the principal low-frequency stability mechanisms without retaining every switching, electromagnetic, and internal-controller state. Although electromagnetic-transient models provide a more detailed representation of converter switching and nonlinear control limits, their complexity may obscure the relationship between individual parameters and modal behaviour. A reduced-order model can therefore complement detailed simulation by providing a transparent basis for parameter sensitivity and physical interpretation.

Battery energy storage systems can provide supplementary support to converter-dominated networks through their power-electronic interfaces. In addition to their conventional energy-management functions, BESS converters can regulate reactive power and support the PCC voltage. This voltage-support function may influence the converter–grid interaction by modifying the voltage deviations observed by the grid-following converter controls [12].

In this study, the BESS operates using reactive-power $Q(U)$ droop control. The BESS converter modifies its reactive-power output in response to deviations in the PCC voltage magnitude. Sustained active-power exchange is limited under the operating conditions considered, while the state of charge evolves on a slower time scale than the retained converter-control dynamics. The BESS is therefore investigated primarily as a supplementary reactive-power and PCC-voltage-support resource rather than as a fast active-power or frequency-response controller.

The influence of BESS inclusion must be distinguished from the effects of grid strength and converter synchronisation. A comparison between cases with and without the BESS can indicate whether the voltage-support controller modifies the retained modal characteristics. However, this comparison does not establish an optimum BESS droop gain or a general expansion of the stable operating region. Such conclusions would require systematic variation of the BESS control parameters and further nonlinear validation.

This paper investigates the small-signal stability of an offshore wind farm integrated with a weak onshore AC network through a VSC-HVDC transmission system. A reduced-order eight-state model is used to represent the dominant dynamics associated with the offshore grid-forming converter, the onshore PLL, active-power control, DC-link voltage regulation, and BESS reactive-power support.

The main contributions of this paper are summarised as follows:

- An explicit reduced-order state-space formulation is presented for the integrated offshore wind–HVDC–grid–BESS system, including the retained state vector, sparse state-matrix structure, operating-point linearisation, and modal assessment criteria.
- The influence of grid strength is evaluated for SCR $= \{1, 2, 3, 5, 10\}$. The resulting eigenvalues show that the oscillation frequency of the PLL-related mode increases as the grid becomes weaker, while its damping ratio decreases from 0.571 at SCR $= 10$ to 0.285 at SCR $= 1$.
- The sensitivity of the PLL-related mode is evaluated for natural-frequency scaling factors $k_{\text{PLL}} = \{0.5, 1.0, 1.5, 2.0\}$. The oscillation frequency increases from 7.41 Hz to 29.51 Hz, while the calculated damping ratio remains approximately constant at 0.428.
- The effects of GFM control parameters and wind-power loading are examined within the limitations of the retained eight-state model. The GFM-related states are interpreted through their real-mode decay characteristics rather than through a separate GFM oscillatory pair.
- The physical origin of the retained modes is interpreted using eigenvalue locations and state participation factors, with the SOC integrator treated separately from the dynamic converter-control modes.

- The influence of the BESS is evaluated through a comparison between cases with and without reactive-power $Q(U)$ voltage support. The comparison shows that BESS inclusion produces no material change in the principal PLL-related oscillatory mode under the investigated operating condition.

The verified results therefore distinguish two characteristics of the PLL-related oscillatory mode. Grid strength primarily affects the mode's relative damping, whereas PLL natural-frequency scaling primarily affects its oscillation frequency. Within the investigated operating condition, the BESS provides supplementary PCC-voltage support but does not produce material improvement in the damping of the PLL-related mode.

The scope of the study is restricted to local small-signal behaviour around selected steady-state operating points. The reduced-order model does not represent converter switching, current limiting, controller saturation, protection operation, fault ride-through behaviour, or post-fault nonlinear recovery. The results are therefore intended to provide modal insight and parameter-sensitivity interpretation rather than a substitute for nonlinear RMS or electromagnetic-transient validation.

The remainder of the paper is organised as follows. Section 2 describes the system configuration, converter operating roles, reduced-order model, assumptions, and scope. Section 3 presents the operating-point linearisation, eigenvalue-based stability assessment, mode-identification procedure, and parameter-variation methodology. Section 4 examines the influence of SCR and PLL natural-frequency scaling and interprets the associated converter–grid interaction. Section 5 evaluates the role of BESS reactive-power and PCC-voltage support. Finally, Section 6 presents the conclusions and recommendations for future work.

2 System Description and Modelling

2.1 System Configuration

The system considered in this study consists of an aggregated offshore wind farm connected to an onshore AC network through a point-to-point voltage-source-converter-based high-voltage direct-current (VSC-HVDC) transmission link. This configuration is representative of offshore wind applications in which the transmission distance and required controllability make VSC-HVDC technology suitable for bulk power transfer [1], [2].

The offshore wind farm is represented by an aggregated model to retain the dominant system-level dynamics while avoiding the computational complexity associated with modelling individual turbines. This representation is considered sufficient for the reduced-order small-signal analysis undertaken in this study.

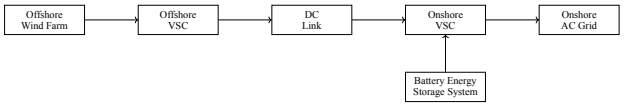


Fig. 1: Configuration of the offshore wind farm connected to the weak onshore AC network through a point-to-point VSC-HVDC link. The BESS is connected on the onshore AC side to provide reactive-power and PCC-voltage support through $Q(U)$ droop control.

Source: Created by the authors.

The overall system configuration is shown in Figure 1. The principal components are the offshore wind farm, offshore VSC, DC transmission link, onshore VSC, weak onshore AC network, and battery energy storage system.

The HVDC transmission system comprises offshore and onshore converters interconnected through the DC link. The offshore converter receives power from the wind-farm collector network and regulates the offshore AC voltage and frequency. The onshore converter transfers the delivered power to the mainland network and regulates the DC-link voltage while synchronising with the onshore AC voltage.

The onshore AC network is represented by a Thevenin equivalent consisting of an ideal voltage source behind an equivalent network impedance. The network strength is parameterised using the short-circuit ratio. Lower SCR values represent weaker-grid conditions and correspond to increased sensitivity of the PCC voltage to converter-current perturbations.

The BESS is connected to the onshore AC side through a voltage-source converter. The BESS converter operates under reactive-power $Q(U)$ droop control and supports the PCC voltage by modifying its reactive-power output in response to voltage deviations. Sustained active-power exchange is limited under the operating conditions considered, while the BESS state of charge evolves on a slower time scale than the converter-control dynamics.

The DC link provides electrical decoupling between the offshore and onshore AC networks. However, the two converter stations remain dynamically coupled through transmitted active power, DC-link voltage variations, and the associated converter control loops. These interactions are retained at a reduced order in the small-signal model presented in Section 2.3.

2.2 Converter Operating Roles and Control Structure

The offshore and onshore VSCs perform different control functions because they interface with electrically distinct AC systems. The offshore converter supplies the offshore collector network, while the onshore converter transfers the generated power to the mainland AC network through a grid-following control structure.

The offshore converter operates in grid-forming mode and establishes the voltage magnitude and frequency of the offshore AC network. Since the offshore collector system does not contain an externally stiff AC voltage source, the offshore VSC provides the voltage and frequency references required by the aggregated wind farm. Its dominant low-frequency behaviour is represented in the reduced-order model by the GFM frequency and voltage-control states, $\Delta\omega_{\text{gfm}}$ and Δv_{gfm}.

The grid-forming control incorporates droop-related damping and virtual-inertia characteristics. Within the retained eight-state formulation, these controls influence the decay characteristics of the GFM-related real modes. A separate GFM virtual-angle state is not retained. Consequently, the adopted model does not represent a distinct GFM swing-mode complex-conjugate pair.

The onshore converter operates in grid-following mode and uses a phase-locked loop to synchronise its rotating reference frame with the onshore AC voltage [9], [13]. The PLL estimates the PCC-voltage angle and provides the phase reference required by the converter current and outer control loops.

The retained PLL states are the angle deviation, $\Delta\theta_{\text{pll}}$, and the frequency-related state, $\Delta\omega_{\text{pll}}$. These states form the principal complex-conjugate mode investigated in the SCR and PLL-bandwidth sensitivity studies. Their dynamic behaviour is influenced by both the PLL controller parameters and the sensitivity of the PCC voltage to converter-current perturbations.

The onshore converter employs a cascaded control structure consisting of fast inner current-control loops and slower outer control loops. The outer DC-link voltage controller maintains the active-power balance between the offshore and onshore converter stations by generating the corresponding d-axis current reference. The reactive-power or AC-voltage controller generates the q-axis current reference.

The inner current controllers regulate the converter currents in the synchronously rotating dq reference frame. The d-axis current is primarily associated with active-power transfer and DC-link voltage regulation, while the q-axis current is primarily associated with reactive-power exchange and AC-voltage support.

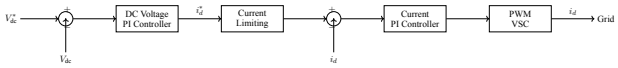


Fig. 2: Cascaded control structure of the grid-following onshore VSC, showing the outer DC-link voltage controller, current-reference limiting, and inner d-axis current-control loop.

Source: Created by the authors.

Figure 2 illustrates the cascaded DC-link voltage and inner current-control structure considered for the grid-following onshore converter.

The inner current-control loops operate on a substantially faster time scale than the outer DC-link, active-power, PLL, GFM, and BESS control dynamics. The detailed current-controller states are therefore not retained explicitly in the reduced-order model. Their influence is represented through the assumption of stable and sufficiently fast current tracking.

The filtered active-power-control state, Δp_f, represents the slower active-power measurement and control behaviour relevant to the DC-link dynamics. The DC-link voltage state, Δv_{dc}, captures the energy imbalance between the offshore and onshore converter stations.

The BESS converter is controlled separately from the onshore HVDC converter. The BESS $Q(U)$ droop controller modifies reactive-power output in response to PCC-voltage deviations and thereby provides supplementary local voltage support. The resulting BESS reactive-power state, Δq_{bess}, and the slow SOC state are included in the reduced-order model developed in Section 2.3.

The distinct operating roles of the offshore GFM converter, onshore grid-following converter, DC-link controller, and BESS voltage-support controller provide the physical basis for the state selection and coupling structure introduced in the following subsection.

2.3 Small-Signal Model Development

A reduced-order small-signal model is developed by linearising the system dynamics around a steady-state operating point [5], [10]. The model retains the dominant low-frequency states associated with the offshore grid-forming converter, onshore PLL, active-power control, DC-link voltage regulation, and BESS reactive-power support.

The small-signal state vector is defined as

$$\Delta\mathbf{x} = \begin{bmatrix}\Delta\mathbf{x}_{\text{gfm}}^T & \Delta\mathbf{x}_{\text{pll}}^T & \Delta\mathbf{x}_{\text{aux}}^T\end{bmatrix}^T, \qquad (1)$$

where

$$\Delta \mathbf{x}_{\text{gfm}} = [\Delta\omega_{\text{gfm}} \quad \Delta v_{\text{gfm}}]^T, \tag{2}$$

$$\Delta \mathbf{x}_{\text{pll}} = [\Delta\theta_{\text{pll}} \quad \Delta\omega_{\text{pll}}]^T, \tag{3}$$

$$\Delta \mathbf{x}_{\text{aux}} = [\Delta p_f \quad \Delta v_{\text{dc}} \quad \Delta\text{SOC} \quad \Delta q_{\text{bess}}]^T. \tag{4}$$

The variables $\Delta\omega_{\text{gfm}}$ and Δv_{gfm} represent the offshore GFM frequency and voltage-control states. The variables $\Delta\theta_{\text{pll}}$ and $\Delta\omega_{\text{pll}}$ represent the onshore PLL angle and frequency states. The auxiliary states comprise the filtered active-power state, Δp_f; DC-link voltage deviation, Δv_{dc}; BESS state-of-charge deviation, ΔSOC; and BESS reactive-power-control state, Δq_{bess}. Following linearisation, the autonomous small-signal system is written as

$$\Delta\dot{\mathbf{x}} = \mathbf{A}(\boldsymbol{\rho})\Delta\mathbf{x}, \tag{5}$$

where $\mathbf{A}$ is the state matrix and $\boldsymbol{\rho}$ denotes the investigated network, controller, and operating-point parameters. Using the state ordering defined in (1), the retained state matrix is

$$\mathbf{A} = \begin{bmatrix} a_{11} & 0 & a_{13} & 0 & 0 & a_{16} & 0 & 0 \\ 0 & a_{22} & a_{23} & 0 & 0 & 0 & 0 & 0 \\ 0 & 0 & 0 & a_{34} & 0 & 0 & 0 & a_{38} \\ 0 & 0 & a_{43} & a_{44} & 0 & 0 & 0 & 0 \\ 0 & 0 & 0 & 0 & a_{55} & 0 & 0 & 0 \\ a_{61} & 0 & 0 & 0 & a_{65} & a_{66} & 0 & 0 \\ 0 & 0 & 0 & 0 & 0 & 0 & 0 & 0 \\ 0 & 0 & a_{83} & 0 & 0 & 0 & 0 & a_{88} \end{bmatrix}. \tag{6}$$

The principal diagonal and PLL coefficients are

$$a_{11} = -\frac{D_{\text{gfm}}}{M_{\text{gfm}}}, \qquad a_{22} = -\frac{1}{T_v}, \tag{7}$$

$$a_{34} = 1 + \frac{K_{v,\text{pll}}}{\text{SCR}}, \qquad a_{43} = -\omega_{\text{pll},n}^2 - \frac{K_{\text{pll},v}}{\text{SCR}}, \tag{8}$$

$$a_{44} = -2\zeta_{\text{pll}}\omega_{\text{pll},n}, \quad a_{55} = -\frac{1}{T_p}, \tag{9}$$

$$a_{66} = -\frac{R_{\text{dc}}}{C_{\text{dc}}}, \qquad a_{88} = -\frac{1}{T_q}. \tag{10}$$

The grid-strength-dependent GFM coupling terms are represented by

$$a_{13} = a_{23} = -\frac{K_{\text{g}}}{\text{SCR}}, \tag{11}$$

where K_{g} is the reduced coupling coefficient between the retained PLL and GFM states. The DC-link coupling terms are represented by

$$a_{16} = K_{\text{dc,gfm}}, \qquad a_{61} = K_{\text{gfm,dc}}, \tag{12}$$

$$a_{65} = K_{\text{wind,dc}} k_{\text{wind}}, \tag{13}$$

where k_{wind} is the wind-loading factor. The term a_{65} represents the retained influence of filtered active-power variations on the DC-link voltage dynamics. The BESS voltage-support coupling is represented by

$$a_{38} = K_{\text{bess},v}, \qquad a_{83} = -K_{v,\text{bess}}, \tag{14}$$

where the signs follow the voltage and reactive-power conventions adopted in the reduced-order model. These terms represent the interaction between the retained PCC-voltage or PLL dynamics and the BESS reactive-power-control state. The BESS reactive-power-control pole is determined by the controller time constant T_q. The corresponding control function is associated with reactive-power $Q(U)$ droop support. The SOC state is represented as a slow integrator:

$$\Delta\dot{\text{SOC}} \simeq 0. \tag{15}$$

The resulting pole at the origin represents slow energy accumulation and is treated separately from the converter-control modes during the stability assessment. The PLL natural frequency is varied according to

$$\omega_{\text{pll},n} = k_{\text{PLL}}\omega_{\text{pll},0}, \tag{16}$$

where k_{PLL} is the dimensionless scaling factor and $\omega_{\text{pll},0}$ is the nominal PLL natural frequency. The complete parameter set may therefore be written as

$$\boldsymbol{\rho} = [\text{SCR}, k_{\text{PLL}}, k_D, k_M, k_{\text{wind}}, \gamma_{\text{BESS}}]^T, \tag{17}$$

where k_D and k_M are the GFM droop-related damping and virtual- inertia scaling factors, respectively. The parameter γ_{BESS} indicates whether the BESS subsystem and its associated voltage-support coupling are included. The coupling coefficients in (6) are reduced-order coefficients used to represent the retained subsystem interactions. They should not be interpreted as universal converter parameters because their numerical values depend on the adopted per-unit bases, controller definitions, network representation, and selected operating point. The model retains the dynamics required for the SCR, PLL scaling, GFM-control, wind-loading, and BESS inclusion studies while excluding high-frequency switching and detailed inner-current-controller states. Within this formulation, the PLL states form the principal complex-conjugate pair, while the GFM, active-power-control, DC-link, BESS, and SOC states contribute primarily to real modes.

2.4 Modelling Assumptions

The reduced-order model is intended to retain the dominant low-frequency dynamics required for local

small-signal stability analysis while maintaining analytical transparency. The following assumptions are adopted:

- The system initially operates at a balanced three-phase steady-state equilibrium. The perturbations considered are sufficiently small for the first-order linearised model to provide a valid representation of the local system dynamics.
- The offshore wind farm is represented by an aggregated model. The individual turbines are assumed to experience comparable operating conditions, and turbine-level electromagnetic dynamics are not retained explicitly.
- The offshore converter operates in grid-forming mode and establishes the offshore AC voltage magnitude and frequency. Its dominant low-frequency behaviour is represented by the GFM frequency and voltage-control states.
- The onshore converter operates in grid-following mode and uses a second-order PLL for grid synchronisation. The retained PLL angle and frequency states form the principal complex-conjugate mode examined in the SCR and PLL scaling studies.
- The voltage-source converters are represented using averaged fundamental-frequency models. Semiconductor switching, pulse-width modulation, and high-frequency electromagnetic transients are neglected.
- The converter inner current-control loops are assumed to be stable and substantially faster than the retained PLL, GFM, active-power, DC-link, and BESS control dynamics. Their detailed states are therefore not included in the reduced-order model.
- All converter control systems operate within their linear regions. Current limiting, modulation saturation, converter blocking, protection operation, and nonlinear control-mode transitions are not represented.
- The onshore AC network is represented by a Thevenin equivalent. Grid strength is parameterised using the SCR, with lower SCR values representing weaker-grid conditions and greater PCC-voltage sensitivity to converter-current perturbations.
- The DC link provides electrical decoupling between the offshore and onshore AC networks. The converter stations nevertheless remain dynamically coupled through active-power transfer, DC-link voltage variations, and their associated control loops.
- The BESS is connected to the onshore AC network through a voltage-source converter operating under reactive-power $Q(U)$ droop control. The BESS therefore provides supplementary reactive-power and PCC-voltage support.
- Sustained BESS active-power exchange is limited under the operating conditions considered. The SOC consequently evolves on a slower time scale than the retained converter-control modes and is represented as an integrator.
- Detailed electrochemical, thermal, ageing, and cell-balancing dynamics of the battery are outside the scope of the reduced-order model.
- Wind-power loading influences the retained active-power and DC-link coupling. The analysis does not include detailed aerodynamic, shaft, pitch-control, or turbine-level electromechanical states.
- The analysis is restricted to local small-signal stability. Large disturbances, AC and DC faults, fault ride-through behaviour, post-fault recovery, and nonlinear time-domain performance are not considered.

2.5 Scope of the Model

The reduced-order model is intended to capture the dominant low-frequency mechanisms relevant to the local small-signal stability of the integrated offshore wind–HVDC–grid–BESS system. The model retains the states required to examine the influence of grid strength, PLL tuning, GFM control characteristics, active-power and DC-link dynamics, wind-power loading, and BESS reactive-power support.

The formulation is not intended to reproduce the complete electromagnetic behaviour of the converters, HVDC link, wind turbines, or battery system. Switching dynamics, detailed inner current-controller states, nonlinear control limits, protection functions, and detailed battery electrochemical dynamics are excluded from the retained state-space representation.

Within the adopted eight-state formulation, the onshore PLL angle and frequency states form the principal complex-conjugate mode. The offshore GFM frequency and voltage states, filtered active-power state, DC-link voltage state, and BESS reactive-power-control state contribute primarily to real modes over the investigated parameter range.

The SOC state is represented as a slow integrator and is treated separately from the dynamic modes used to assess local stability.

The model is used to evaluate discrete variations in SCR, PLL natural-frequency scaling, GFM droop-related damping, virtual inertia, wind-power loading, and BESS inclusion. The resulting eigenvalue locations, oscillation frequencies, damping ratios, and state participation factors are used to interpret the corresponding modal behaviour.

The calculated trends apply only to the investigated parameter values and selected steady-state operating conditions. The results are not used to establish a universal critical SCR, maximum permissible PLL bandwidth, optimum BESS droop gain, or closed-form stability boundary.

Large-disturbance stability, converter-current limiting, control saturation, AC and DC faults, fault ride-through behaviour, and post-fault recovery require nonlinear RMS or electromagnetic-transient analysis and are outside the scope of this study.

Subject to these limitations, the retained model provides a transparent and computationally efficient framework for identifying the principal modal sensitivities of the studied system. The eigenvalue-based assessment methodology applied to this model is presented in Section 3.

3 Small-Signal Stability Analysis Methodology

3.1 Operating Point and Linearisation

The small-signal stability analysis is performed around a steady-state operating point representing nominal power transfer from the offshore wind farm to the onshore AC network through the VSC-HVDC transmission link [3], [5]. At this operating point, the converter control loops operate within their linear regions, the DC-link voltage is regulated around its reference value, and the BESS operates under reactive-power $Q(U)$ droop control. The nonlinear dynamic model can be expressed in the general form

$$\dot{\mathbf{x}} = \mathbf{f}\left(\mathbf{x}, \mathbf{u}, \boldsymbol{\rho}\right), \tag{18}$$

where $\mathbf{x}$ is the system state vector, $\mathbf{u}$ is the external input and disturbance vector, and $\boldsymbol{\rho}$ is the parameter vector defined in (17). The selected equilibrium point, $(\mathbf{x}_0, \mathbf{u}_0, \boldsymbol{\rho}_0)$, satisfies

$$\mathbf{f}\left(\mathbf{x}_0, \mathbf{u}_0, \boldsymbol{\rho}_0\right) = \mathbf{0}. \tag{19}$$

Small perturbations around the equilibrium point are defined as

$$\Delta\mathbf{x} = \mathbf{x} - \mathbf{x}_0, \tag{20}$$

$$\Delta\mathbf{u} = \mathbf{u} - \mathbf{u}_0. \tag{21}$$

Applying a first-order Taylor-series expansion to (18) around the equilibrium point gives

$$\Delta\dot{\mathbf{x}} = \mathbf{A}\Delta\mathbf{x} + \mathbf{B}\Delta\mathbf{u}, \tag{22}$$

where the state and input matrices are obtained from the corresponding Jacobians:

$$\mathbf{A} = \left.\frac{\partial \mathbf{f}}{\partial \mathbf{x}}\right|_0, \tag{23}$$

$$\mathbf{B} = \left.\frac{\partial \mathbf{f}}{\partial \mathbf{u}}\right|_0. \tag{24}$$

The subscript 0 denotes evaluation at $(\mathbf{x}_0, \mathbf{u}_0, \boldsymbol{\rho}_0)$. The modal analysis considers the unforced response of the system following a small perturbation. Setting $\Delta\mathbf{u} = \mathbf{0}$ reduces (22) to

$$\Delta\dot{\mathbf{x}} = \mathbf{A}\Delta\mathbf{x}, \tag{25}$$

which is consistent with the reduced-order state-space formulation in (5). For each sensitivity study, the parameter under investigation is varied while the remaining model parameters are maintained at their base-case values. The corresponding entries of the state matrix are then updated before the eigenvalues and modal quantities are recalculated. Grid-strength variation is introduced through the SCR-dependent entries of the state matrix. PLL sensitivity is evaluated by changing the natural-frequency scaling factor k_{PLL}. The GFM droop-related damping factor, virtual-inertia factor, wind-loading factor, and BESS inclusion parameter are varied through their corresponding entries in $\boldsymbol{\rho}$. The steady-state operating point is maintained during each individual parameter study to isolate the effect of the selected parameter on the retained modal characteristics. The resulting eigenvalue migration is therefore interpreted as the local sensitivity of the linearised model to the investigated network, controller, or operating-condition variation.

3.2 Eigenvalue-Based Stability Assessment

The local small-signal stability of the linearised system is evaluated from the eigenvalues of the state matrix $\mathbf{A}$. The eigenvalues are obtained from the characteristic equation

$$\det\left(\lambda\mathbf{I} - \mathbf{A}\right) = 0, \tag{26}$$

where λ is a system eigenvalue and $\mathbf{I}$ is the identity matrix of appropriate dimension. Each eigenvalue can be expressed as

$$\lambda_i = \sigma_i + j\omega_i, \tag{27}$$

where σ_i is the real part and ω_i is the imaginary part of the ith eigenvalue. The real part determines the

exponential decay or growth of the corresponding modal response, while the imaginary part determines its oscillatory behaviour. For a complex-conjugate eigenvalue pair, the undamped natural frequency is calculated as

$$\omega_{n,i} = \sqrt{\sigma_i^2 + \omega_i^2}, \tag{28}$$

and the corresponding damping ratio is

$$\zeta_i = -\frac{\sigma_i}{\omega_{n,i}}. \tag{29}$$

The oscillation frequency expressed in hertz is

$$f_i = \frac{|\omega_i|}{2\pi}. \tag{30}$$

The linearised system is locally asymptotically stable when all non-integrator eigenvalues satisfy

$$\mathrm{Re}\,(\lambda_i) < 0. \tag{31}$$

An eigenvalue with a positive real part represents an unstable mode, whereas an eigenvalue with a negative real part represents a decaying mode. An eigenvalue located closer to the imaginary axis has a slower decay rate than one located further into the left-half plane.

Real eigenvalues correspond to non-oscillatory modes. Complex- conjugate eigenvalue pairs represent oscillatory modes and are assessed using their real parts, oscillation frequencies, and damping ratios. A reduction in damping ratio does not necessarily require a rightward eigenvalue shift because the damping ratio depends on both the real and imaginary components of the mode.

This distinction is important for the SCR sensitivity results. In that study, the real part of the PLL-related oscillatory pair remains approximately constant, while the imaginary component increases as the SCR decreases. The resulting increase in oscillation frequency therefore reduces the damping ratio even though the eigenvalue pair does not move substantially toward the imaginary axis.

The BESS SOC equation introduces an expected integrator mode at, or numerically close to, the origin. This mode represents the slow accumulation of stored energy and is not interpreted as an oscillatory instability. The SOC integrator is therefore excluded when identifying the critical dynamic eigenvalue.

For each parameter variation, the complete eigenvalue spectrum is calculated. After excluding the expected SOC integrator, the critical dynamic eigenvalue, denoted by λ_{crit}, is defined as the eigenvalue having the largest real part. This mode has the slowest decay rate among the retained non-integrator modes.

The principal oscillatory mode is identified separately as the complex-conjugate eigenvalue pair having the largest real part among the oscillatory modes. Distinguishing the critical dynamic eigenvalue from the principal oscillatory mode prevents a slowly decaying real mode from being incorrectly treated as the dominant oscillatory pair.

The decay margin associated with the critical dynamic eigenvalue is defined as

$$m_\sigma = -\,\mathrm{Re}\,(\lambda_{\text{crit}})\,. \tag{32}$$

A larger positive value of m_σ indicates a faster decay of the critical dynamic mode, while $m_\sigma \to 0$ indicates that the mode is approaching the small-signal stability boundary.

The damping ratio is used specifically to assess oscillatory modes, whereas m_σ describes the decay margin of the critical dynamic eigenvalue. These quantities are not interchangeable because the critical dynamic mode may be real while the principal oscillatory mode is a complex-conjugate pair.

3.3 Dominant Mode Identification

The critical dynamic eigenvalue and principal oscillatory mode are identified using the criteria defined in Section 3.2. The critical dynamic eigenvalue is the non-integrator eigenvalue having the largest real part, while the principal oscillatory mode is the complex-conjugate pair having the largest real part among the oscillatory modes.

The physical origin of each mode is assessed using the associated right and left eigenvectors. For the ith eigenvalue, these eigenvectors satisfy

$$\mathbf{A}\boldsymbol{\phi}_i = \lambda_i \boldsymbol{\phi}_i, \tag{33}$$

$$\boldsymbol{\psi}_i^T \mathbf{A} = \lambda_i \boldsymbol{\psi}_i^T, \tag{34}$$

where $\boldsymbol{\phi}_i$ and $\boldsymbol{\psi}_i$ are the right and left eigenvectors associated with λ_i, respectively. The participation of the kth state in the ith mode is estimated from

$$p_{ki} = |\phi_{ki}\psi_{ik}|\,, \tag{35}$$

where ϕ_{ki} is the kth element of the right eigenvector and ψ_{ik} is the corresponding element of the left eigenvector. For comparison between states, the participation factors are normalised according to

$$\bar{p}_{ki} = \frac{p_{ki}}{\sum_{r=1}^{n} p_{ri}}, \tag{36}$$

where $n = 8$ is the number of retained states. The normalised participation factors satisfy

$$\sum_{k=1}^{n} \bar{p}_{ki} = 1. \tag{37}$$

Using the state ordering defined in (1), the retained states are grouped into four subsystems:

- the offshore GFM subsystem, represented by $\Delta\omega_{\text{gfm}}$ and Δv_{gfm};
- the onshore PLL subsystem, represented by $\Delta\theta_{\text{pll}}$ and $\Delta\omega_{\text{pll}}$;
- the active-power and DC-link subsystem, represented by Δp_f and Δv_{dc}; and
- the BESS subsystem, represented by ΔSOC and Δq_{bess}.

The contribution of subsystem s to mode i is determined by summing the normalised participation factors of the states belonging to that subsystem:

$$P_{s,i} = \sum_{k \in \mathcal{S}_s} \bar{p}_{ki}, \tag{38}$$

where $\mathcal{S}_s$ denotes the set of state indices associated with subsystem s.

A mode is interpreted as being associated predominantly with the subsystem having the largest aggregated participation. Where two subsystems have comparable contributions, the mode is interpreted as an interaction mode rather than being assigned exclusively to one control subsystem.

For the parameter studies presented in Section 4, the principal complex-conjugate pair is associated with the retained PLL angle and frequency states. This pair is therefore referred to as the PLL-related oscillatory mode. Its identification is also supported by its strong sensitivity to the PLL natural-frequency scaling factor.

The GFM frequency and voltage-control states contribute primarily to real eigenvalues within the adopted eight-state formulation. These modes are interpreted as GFM-related real modes describing non-oscillatory decay. They are not treated as a separate GFM oscillatory pair because a GFM virtual-angle state is not retained in the model.

The filtered active-power and DC-link voltage states similarly contribute primarily to real modes associated with power-control and DC-link energy-balancing dynamics. The BESS reactive-power state is associated with the $Q(U)$ voltage-support controller, while the SOC state produces the expected integrator mode at the origin.

The participation-factor assessment is used principally to support the physical classification of the retained modes. The conclusions are based on the combined evidence from eigenvalue location, parameter sensitivity, and state association rather than on an unsupported numerical participation threshold.

3.4 Parameter Variation and Sensitivity Analysis

A systematic parameter-variation study is performed to evaluate the influence of grid strength, converter-control parameters, wind-power loading, and BESS inclusion on the eigenstructure of the reduced-order model. During each study, the parameter under investigation is varied while the remaining parameters are maintained at their base-case values.

For every parameter value, the state matrix is reconstructed and the complete eigenvalue spectrum is calculated. The critical dynamic eigenvalue, principal oscillatory mode, damping ratio, oscillation frequency, and decay margin are then evaluated using the criteria defined in Sections 3.2 and 3.3.

Grid strength is varied through the SCR of the onshore AC network:

$$\text{SCR} \in \{1,\ 2,\ 3,\ 5,\ 10\}\,. \tag{39}$$

These values represent operating conditions ranging from a very weak grid to a comparatively strong grid. The SCR-dependent entries of the state matrix are updated at each operating point.

PLL sensitivity is evaluated by scaling the nominal PLL natural frequency according to

$$\omega_{\text{pll},n} = k_{\text{PLL}}\omega_{\text{pll},0}, \tag{40}$$

where $\omega_{\text{pll},0}$ is the nominal PLL natural frequency. The investigated scaling factors are

$$k_{\text{PLL}} \in \{0.5,\ 1.0,\ 1.5,\ 2.0\}\,. \tag{41}$$

The SCR and PLL studies are interpreted separately because the verified results show different sensitivities. Variation of SCR changes the oscillation frequency and damping ratio of the PLL-related mode, while variation of k_{PLL} primarily changes its oscillation frequency. The PLL scaling study does not produce a material change in damping ratio over the investigated range.

The GFM droop-related damping factor is varied over

$$k_D \in \{0.5,\ 1.0,\ 2.0,\ 3.0\}\,, \tag{42}$$

and the GFM virtual-inertia scaling factor is varied according to

$$k_M \in \{0.5,\ 1.0,\ 2.0,\ 3.0\}\,. \tag{43}$$

Within the retained eight-state formulation, the offshore GFM frequency and voltage states are represented by first-order dynamics. The GFM studies are therefore used to assess changes in the decay characteristics of the corresponding real modes.

They are not interpreted as sensitivity studies of a separate GFM complex-conjugate mode.

The influence of offshore wind-power transfer is represented by the wind-loading factor

$$k_{\text{wind}} \in \{0,\ 0.5,\ 1.0,\ 1.5\}\,. \tag{44}$$

This factor modifies the retained coupling between the filtered active-power state and the DC-link voltage state. The study evaluates whether changes in wind-power loading materially affect the retained modal characteristics.

The influence of BESS voltage support is assessed using two configurations. The first includes the BESS SOC state, reactive-power-control state, and voltage-support coupling. The second excludes the BESS states and their associated coupling. The remaining network, converter-control, DC-link, and operating-point parameters are maintained at the same values.

The BESS assessment is therefore a comparison between cases with and without reactive-power $Q(U)$ voltage support. It is not a multi-value sensitivity study of the BESS droop gain K_{QU}. Accordingly, the comparison cannot be used to identify an optimum BESS gain or establish a general relationship between BESS gain and modal damping.

Eigenvalues at consecutive parameter values are compared using their locations in the complex plane. For a mode identified at parameter value ρ_j, the distance to a candidate mode at the following parameter value is defined as

$$d_{ik} = |\lambda_i(\rho_j) - \lambda_k(\rho_j + \Delta\rho_j)|\,. \tag{45}$$

The candidate eigenvalue having the smallest distance is treated as the continuation of the modal branch. Where modes are closely spaced, their associated state participation is also considered to reduce the risk of incorrect mode matching.

The sensitivity assessment is based on eigenvalue migration between the investigated discrete parameter values rather than on a claimed closed-form derivative of every state-matrix entry. For each oscillatory mode, changes in the real part, imaginary part, oscillation frequency, and damping ratio are evaluated together.

A change in damping ratio is not interpreted solely from horizontal eigenvalue movement because the damping ratio depends on both the real and imaginary components. This distinction is particularly important for the SCR study, where the damping ratio changes while the real part of the PLL-related mode remains approximately constant.

The parameter studies provide local sensitivity information for the selected operating point and retained model structure. The results are not extrapolated beyond the investigated ranges and are not used to define universal controller settings or stability boundaries.

3.5 Interpretation Framework

The eigenvalue results are interpreted by considering the real part, imaginary part, oscillation frequency, damping ratio, decay margin, and state participation of each retained mode. This combined approach distinguishes changes in modal frequency from changes in modal decay and prevents damping behaviour from being inferred solely from horizontal eigenvalue movement.

The real part of an eigenvalue determines the exponential decay or growth of the corresponding mode. For a stable mode, a more negative real part indicates faster modal decay. The imaginary part determines the oscillation frequency of a complex-conjugate mode.

The damping ratio depends on both the real and imaginary components of the eigenvalue:

$$\zeta_i = -\frac{\sigma_i}{\sqrt{\sigma_i^2 + \omega_i^2}}. \tag{46}$$

Consequently, the damping ratio may decrease even when the real part remains approximately constant if the magnitude of the imaginary component increases. Conversely, the real and imaginary components may both increase in magnitude while the damping ratio remains nearly constant if they change in approximately the same proportion.

This distinction is applied directly to the SCR and PLL sensitivity studies. During the SCR variation, the real part of the PLL-related mode remains approximately constant, while the imaginary component increases as the grid becomes weaker. The resulting increase in modal frequency causes the damping ratio to decrease.

During the PLL scaling study, the magnitudes of the real and imaginary components increase in approximately the same proportion. The oscillation frequency consequently increases substantially, while the damping ratio remains nearly constant. The PLL scaling result is therefore interpreted as modal-frequency sensitivity rather than progressive damping degradation.

The physical origin of each mode is assessed using the state participation framework described in Section 3.3. The principal complex-conjugate pair is associated with the retained PLL angle and frequency states and is therefore interpreted as the PLL-related oscillatory mode.

Modes associated primarily with the offshore GFM frequency and voltage states are interpreted as GFM-related real modes. Within the adopted

eight-state formulation, these states are represented by first-order dynamics and do not form a separate GFM complex-conjugate pair. Accordingly, the effects of GFM droop and virtual inertia are interpreted through changes in real-mode decay characteristics.

The filtered active-power and DC-link voltage states are interpreted as non-oscillatory power-control and energy-balancing modes. The BESS reactive-power state represents the dynamic response of the $Q(U)$ voltage-support controller, while the SOC state produces the expected integrator mode at the origin.

The SOC integrator is treated separately from the dynamic modes used to assess local stability. Its location at the origin represents slow energy accumulation rather than an oscillatory converter-control instability.

The BESS comparison is interpreted using the calculated eigenvalue difference between cases with and without reactive-power voltage support. The comparison does not show a material change in the principal PLL-related oscillatory mode. The BESS is therefore interpreted primarily as a supplementary PCC-voltage-support resource rather than as a source of significant modal-damping enhancement.

The interpretation is restricted to the investigated discrete parameter values and selected steady-state operating conditions. Numerical trends are not extrapolated beyond the analysed ranges and are not used to establish universal controller settings, stability thresholds, or closed-form stability boundaries.

Within these limitations, the framework provides a transparent basis for relating the calculated eigenvalue characteristics to grid strength, PLL tuning, GFM control parameters, DC-link dynamics, wind-power loading, and BESS reactive-power support.

4 Impact of Grid Strength and PLL Bandwidth on Stability

4.1 Effect of Grid Strength on Small-Signal Stability

The influence of grid strength on the small-signal stability of the HVDC-connected offshore wind system is investigated by varying the short-circuit ratio of the onshore AC network over SCR $= \{1, 2, 3, 5, 10\}$. The remaining network, converter, DC-link, BESS, and operating-point parameters are maintained at their base-case values. This approach isolates the influence of onshore grid strength on the eigenstructure of the reduced-order model.

Figure 3 presents the selected PLL-related complex-conjugate eigenvalue pair for the investigated SCR values. The horizontal and vertical axes represent the real part, σ, in s^{-1} and the imaginary part, ω, in rad/s, respectively. The vertical line at $\mathrm{Re}(\lambda) = 0$ represents the small-signal stability boundary.

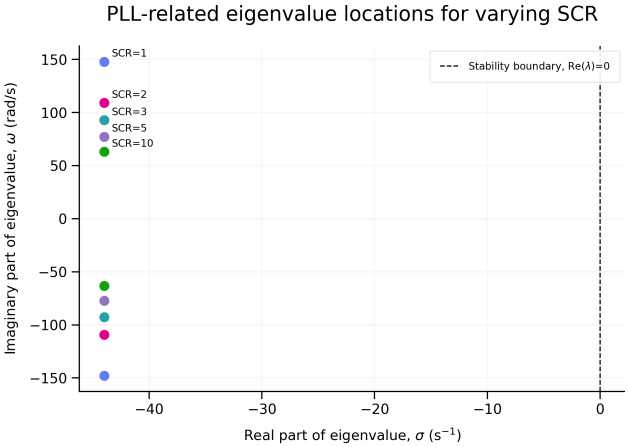


Fig. 3: PLL-related eigenvalue locations for SCR $= \{1, 2, 3, 5, 10\}$ at the nominal PLL setting. Lower SCR increases the modal frequency and reduces the damping ratio, while the real part remains approximately constant. The dashed line denotes the small-signal stability boundary, $\mathrm{Re}(\lambda) = 0$.

Source: Created by the authors.

Table 1. Representative PLL-Related Modal Results for the SCR Sensitivity Study

SCR	λ_{osc} (s^{-1})	f (Hz)	ζ
1	$-43.98 + j147.89$	23.54	0.285
2	$-43.98 + j109.17$	17.37	0.374
3	$-43.98 + j92.80$	14.77	0.428
5	$-43.98 + j77.26$	12.30	0.495
10	$-43.98 + j63.17$	10.05	0.571

Source: Created by the authors.

Table 1 provides representative numerical results for the PLL-related oscillatory mode. The real part remains approximately constant at -43.98 s^{-1} over the investigated SCR range, while the magnitude of the imaginary part decreases as the grid becomes stronger. Consequently, the oscillation frequency decreases from 23.54 Hz at SCR $= 1$ to 10.05 Hz at SCR $= 10$, while the damping ratio increases from 0.285 to 0.571.

The calculated eigenvalue spectrum contains a complex-conjugate mode associated predominantly with the retained onshore PLL states, together with real modes associated with the offshore GFM, active-power-control, DC-link, and BESS dynamics. The SOC integrator at the origin is excluded from the assessment of the critical dynamic mode.

As the SCR is reduced, the imaginary component and oscillation frequency of the PLL-related mode

increase, while its real part remains approximately constant over the investigated range. The resulting damping ratio decreases as the grid becomes weaker. Conversely, increasing the SCR reduces the modal frequency and increases the damping ratio. This trend confirms that the PLL-related mode becomes more sensitive to converter–grid interaction as the onshore network weakens [9], [10].

The physical basis of this behaviour is the increased sensitivity of the PCC voltage to converter-current perturbations under weak-grid conditions. These voltage perturbations enter the PLL synchronisation loop and modify the effective feedback between converter phase, current, and network voltage. The interaction is therefore stronger at lower SCR values and weaker when the grid is comparatively stiff.

The SCR variation has a smaller influence on the modes associated with the active-power filter and DC-link voltage than on the PLL-related oscillatory pair. This indicates that, within the adopted reduced-order formulation, grid strength primarily affects the converter synchronisation dynamics rather than uniformly shifting the complete eigenvalue spectrum.

The results demonstrate a clear qualitative relationship between network strength and modal damping. However, the discrete SCR values investigated in this study are not used to establish a universal critical SCR threshold. Such a threshold would depend on the selected converter ratings, controller parameters, network impedance characteristics, and operating point. The results are therefore interpreted within the parameter range and model assumptions adopted for the present study.

4.2 Effect of PLL Bandwidth on Stability Characteristics

The phase-locked loop plays a central role in the dynamic interaction between the grid-following onshore converter and the AC network. Its influence is investigated by varying the PLL natural frequency while maintaining the grid strength and the remaining model parameters at their base-case values.

The PLL natural frequency is varied using the scaling relationship defined in (40), with $k_{\mathrm{PLL}} = \{0.5, 1.0, 1.5, 2.0\}$. These values represent PLL settings ranging from slower synchronisation dynamics to a more aggressive response. The scaling factors are dimensionless and are applied to the nominal PLL natural frequency $\omega_{\mathrm{pll},0}$.

Figure 4 presents the selected PLL-related complex-conjugate eigenvalue pair for the investigated PLL natural-frequency scaling factors. The horizontal axis represents the real part of the eigenvalue, σ, in s^{-1}, while the vertical axis represents the imaginary part, ω, in rad/s. The vertical line at $\mathrm{Re}(\lambda) = 0$ denotes the small-signal stability boundary.

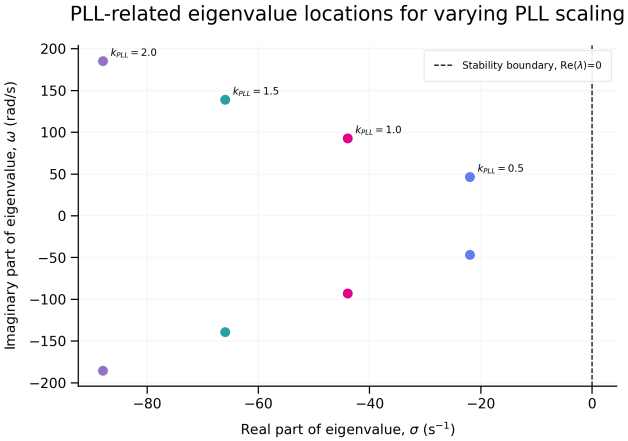


Fig. 4: PLL-related eigenvalue locations for natural-frequency scaling factors $k_{\mathrm{PLL}} = \{0.5, 1.0, 1.5, 2.0\}$. Increasing k_{PLL} increases the modal frequency, while the damping ratio remains approximately constant. The dashed line denotes the small-signal stability boundary, $\mathrm{Re}(\lambda) = 0$.

Source: Created by the authors.

Table 2. Representative PLL-Related Modal Results for the PLL-Bandwidth Sensitivity Study

k_{PLL}	λ_{osc} (s^{-1})	f (Hz)	ζ
0.5	$-21.99 + j46.54$	7.41	0.427
1.0	$-43.98 + j92.80$	14.77	0.428
1.5	$-65.97 + j139.11$	22.14	0.428
2.0	$-87.96 + j185.45$	29.51	0.429

Source: Created by the authors.

Table 2 provides representative numerical results for the PLL-related oscillatory mode. Increasing the PLL natural-frequency scaling factor increases both the magnitude of the real part and the imaginary part of the eigenvalue pair. The oscillation frequency increases from 7.41 Hz at $k_{\mathrm{PLL}} = 0.5$ to 29.51 Hz at $k_{\mathrm{PLL}} = 2.0$. However, the damping ratio remains approximately constant at 0.428 over the investigated range.

The eigenvalue pair having the highest participation from $\Delta\theta_{\mathrm{pll}}$ and $\Delta\omega_{\mathrm{pll}}$ is identified as the PLL-related oscillatory mode. As the PLL scaling factor is increased, the imaginary part of this mode increases, indicating an increase in its oscillation frequency. The remaining real modes exhibit comparatively smaller changes because their dynamics are associated primarily with the GFM, active-power-control, DC-link, and BESS subsystems.

The movement of the PLL-related mode reflects

the increased speed of the synchronisation loop. A faster PLL responds more rapidly to variations in the measured grid voltage angle. Under weak-grid conditions, however, the measured voltage is itself influenced by converter-current perturbations and the network impedance. The PLL therefore interacts with a voltage signal that is more sensitive to the converter response than it would be in a strong network [8], [9], [11].

This interaction introduces an important control-design consideration. Increasing the PLL bandwidth improves the speed of phase tracking and increases the frequency of the PLL-related mode. Although weak-grid PLL interactions may reduce damping in more detailed converter models, the present eight-state formulation produces an approximately constant damping ratio over the investigated PLL scaling range. The result is therefore interpreted as evidence of modal-frequency sensitivity rather than damping degradation.

Within the investigated parameter range, the PLL-related mode shows a clear increase in oscillation frequency as k_{PLL} increases. The eigenvalue pair also moves further into the left-half plane because the magnitude of its real part increases with the PLL scaling factor. However, the real and imaginary components increase in approximately the same proportion, and the damping ratio therefore remains nearly constant. The retained eight-state model consequently demonstrates strong frequency sensitivity to PLL tuning but does not demonstrate a reduction in the damping ratio over the investigated range.

The investigated scaling factors are used to demonstrate the sensitivity of the reduced-order model to PLL tuning. They are not used to establish a universal maximum PLL bandwidth because the allowable tuning range depends on the SCR, converter-control gains, network impedance, operating point, and the definition of the nominal PLL frequency. Accordingly, the results are interpreted only for the model and operating conditions considered in this study.

4.3 Combined Influence of Grid Strength and PLL Bandwidth

The preceding analyses demonstrate that SCR and PLL tuning influence different characteristics of the retained PLL-related oscillatory mode. Grid strength primarily affects the relationship between the modal frequency and damping ratio, while the PLL natural-frequency scaling factor strongly determines the absolute speed of the oscillatory response.

The SCR results in Table 1 show that the real part of the PLL-related eigenvalue remains approximately constant over the investigated range, while its imaginary component increases as the grid becomes weaker. Consequently, the damping ratio decreases from 0.571 at $\mathrm{SCR} = 10$ to 0.285 at $\mathrm{SCR} = 1$.

The PLL-bandwidth results in Table 2 show that increasing k_{PLL} increases both the real and imaginary components of the PLL-related mode in approximately the same proportion. The oscillation frequency therefore increases substantially, while the damping ratio remains nearly constant at approximately 0.428.

These findings indicate that the retained eight-state model exhibits two related but distinct sensitivities. A reduction in SCR increases the frequency of the PLL-related mode relative to its decay rate and therefore reduces its damping ratio. In contrast, an increase in the PLL natural-frequency scaling factor increases the overall speed of the mode without producing a material reduction in its damping ratio over the investigated range.

The combined interpretation can be expressed qualitatively as

$$\mathrm{SCR}\downarrow \quad \Longrightarrow \quad f_{\mathrm{osc}}\uparrow, \qquad \zeta_{\mathrm{osc}}\downarrow, \tag{47}$$

whereas

$$k_{\mathrm{PLL}}\uparrow \quad \Longrightarrow \quad f_{\mathrm{osc}}\uparrow, \qquad \zeta_{\mathrm{osc}} \approx \text{constant}. \tag{48}$$

Equations (47) and (48) summarise the trends obtained from the discrete parameter studies. They should not be interpreted as closed-form stability criteria or as universal relationships applicable to all converter and network configurations.

Although more detailed converter models may exhibit PLL-damping degradation as the bandwidth increases under weak-grid conditions, that behaviour is not demonstrated by the present eight-state results. The calculated results instead demonstrate that weak-grid conditions reduce the damping ratio, while increasing PLL bandwidth primarily increases the modal frequency.

The results nevertheless confirm that PLL tuning should be assessed together with the expected range of grid strengths. A high-frequency PLL mode may impose different control-interaction and implementation requirements even when its calculated damping ratio remains approximately constant. Grid strength, controller bandwidth, measurement filtering, current-control dynamics, and digital-control delays should therefore be considered together during detailed converter design.

The discrete parameter study does not establish a universal critical SCR, a maximum allowable PLL bandwidth, or a combined SCR–PLL stability boundary. Such limits would require a more detailed converter representation and systematic evaluation of additional control, network, and operating-point parameters.

4.4 Physical Interpretation of Dominant Modes

The physical origin of the retained modes is interpreted from their eigenvalue locations, sensitivity to the investigated parameters, and associated state participation. Within the adopted eight-state model, the principal complex-conjugate pair is associated predominantly with the onshore PLL angle and frequency states, $\Delta\theta_{\text{pll}}$ and $\Delta\omega_{\text{pll}}$.

The PLL estimates the PCC-voltage angle and establishes the synchronous reference frame required by the grid-following converter control system. Perturbations in the PCC voltage therefore influence the PLL states and, through the converter control loops, modify the converter current response. The resulting feedback path links the PLL dynamics to the equivalent onshore network impedance.

Under comparatively strong-grid conditions, the PCC voltage is less sensitive to converter-current perturbations. As the SCR decreases, the equivalent network impedance increases and the same current perturbation produces a larger change in the PCC voltage. This strengthens the interaction between the converter synchronisation loop and the weak network [8], [9], [10].

The numerical results in Table 1 show that the real part of the PLL-related eigenvalue pair remains approximately constant as the SCR is varied. However, the imaginary component increases substantially as the grid becomes weaker. The oscillation frequency consequently increases from 10.05 Hz at SCR $= 10$ to 23.54 Hz at SCR $= 1$.

Because the magnitude of the imaginary component increases while the real part remains nearly unchanged, the damping ratio decreases from 0.571 to 0.285. The SCR sensitivity is therefore expressed primarily through an increase in modal frequency relative to the decay rate, rather than through a substantial rightward displacement of the eigenvalue pair.

The PLL-bandwidth results in Table 2 show a different response. Increasing the PLL natural-frequency scaling factor increases both the magnitude of the real part and the imaginary part of the PLL-related mode. These components increase in approximately the same proportion, causing the damping ratio to remain nearly constant at approximately 0.428.

The retained model therefore demonstrates that the PLL scaling factor strongly influences the speed and oscillation frequency of the synchronisation mode. It does not, however, demonstrate progressive damping degradation as the PLL scaling factor increases. Although such degradation may occur in more detailed weak-grid converter models, it is not claimed as a numerical result of the present eight-state formulation.

The observed oscillatory pair is consequently interpreted as a PLL-related converter–grid interaction mode. Its frequency is sensitive to both grid strength and PLL tuning, while its calculated damping ratio is influenced more strongly by the SCR variation than by the PLL scaling variation.

The active-power-control and DC-link voltage states contribute primarily to real modes within the reduced-order model. These modes represent non-oscillatory decay associated with filtered power-control and DC-link energy-balancing dynamics. Their comparatively limited movement during the SCR and PLL studies indicates that they are not the principal source of the oscillatory sensitivity observed in Tables 1 and 2.

The offshore GFM frequency and voltage states are also represented by first-order dynamics in the adopted formulation. Changes in their corresponding real eigenvalues describe variations in modal decay rate and should not be interpreted as a separate GFM oscillatory pair. Accordingly, the effects of GFM droop and virtual inertia are discussed in relation to the retained GFM-related real modes rather than being attributed to the PLL-related complex-conjugate mode.

The BESS reactive-power state influences the retained system through the PCC-voltage-support coupling. When the BESS is included, its $Q(U)$ droop controller responds to PCC-voltage deviations by modifying reactive-power output. The resulting modal influence is limited in comparison with the changes produced by SCR and PLL scaling.

The physical interpretation is therefore restricted to the trends calculated over the investigated discrete parameter values. The reduced-order results identify the PLL synchronisation subsystem as the principal source of oscillatory behaviour, with SCR determining the mode's relative damping characteristics and PLL scaling determining primarily its oscillation frequency.

4.5 Summary of Stability Trends

The SCR and PLL-bandwidth studies identify the onshore converter synchronisation dynamics as the principal source of oscillatory behaviour within the adopted eight-state model. The main findings are summarised as follows:

- The principal complex-conjugate mode is associated predominantly with the onshore PLL angle and frequency states. The remaining GFM, active-power-control, DC-link, SOC, and BESS states contribute primarily to real modes over the investigated parameter range.

- Decreasing the SCR increases the imaginary component and oscillation frequency of the PLL-related mode, while its real part remains approximately constant. The damping ratio consequently decreases as the grid becomes weaker.
- Increasing the SCR reduces the oscillation frequency of the PLL-related mode and increases its damping ratio. The damping ratio increases from 0.285 at SCR $= 1$ to 0.571 at SCR $= 10$.
- Increasing the PLL natural-frequency scaling factor produces a substantial increase in the oscillation frequency of the PLL-related mode. The frequency increases from 7.41 Hz at $k_{\mathrm{PLL}} = 0.5$ to 29.51 Hz at $k_{\mathrm{PLL}} = 2.0$.
- The real and imaginary components of the PLL-related mode increase in approximately the same proportion during the PLL scaling study. The calculated damping ratio therefore remains nearly constant at approximately 0.428 over the investigated range.
- The retained eight-state model demonstrates strong PLL-modal-frequency sensitivity to the selected PLL scaling factor, but it does not demonstrate progressive damping degradation as the PLL scaling factor increases.
- Grid strength and PLL tuning influence different characteristics of the same PLL-related oscillatory mode. SCR primarily affects the mode's relative damping characteristics, whereas PLL scaling primarily determines its oscillation frequency.
- The offshore GFM frequency and voltage states are represented by first-order dynamics. The effects of GFM droop and virtual inertia are therefore interpreted through changes in the decay characteristics of the retained GFM-related real modes rather than through a separate GFM oscillatory eigenvalue pair.
- The active-power-control and DC-link voltage modes exhibit comparatively limited movement during the SCR and PLL studies. This indicates that the principal oscillatory sensitivity is associated with the onshore PLL synchronisation subsystem.
- The investigated parameter variations establish numerical trends for the selected reduced-order model and operating conditions. They do not establish a universal critical SCR, maximum allowable PLL bandwidth, or closed-form combined stability boundary.

Overall, the results demonstrate that decreasing grid strength reduces the damping ratio of the PLL-related mode, while increasing the PLL natural-frequency scaling factor primarily increases its oscillation frequency. These findings show that grid strength and PLL tuning should be assessed together, while recognising that the retained model does not reproduce every weak-grid interaction that may be present in a higher-order converter representation.

The results also show that SCR and PLL scaling have a greater influence on the principal oscillatory mode than the retained active-power, DC-link, and voltage-support dynamics. Section 5 therefore evaluates whether supplementary BESS reactive-power $Q(U)$ voltage support produces a detectable change in the converter–grid modal characteristics under the investigated weak-grid operating condition.

5 Influence of Energy Storage on Voltage Support

5.1 Motivation for Energy Storage as a Stability Resource

The results presented in Section 4 demonstrate that weak-grid conditions increase the sensitivity of the grid-following onshore converter to PLL–grid interactions. The retained model also shows that PLL natural-frequency scaling strongly influences the frequency of the principal oscillatory mode. Supplementary voltage support may therefore be considered as an additional measure for reducing PCC-voltage sensitivity to converter and network perturbations.

Battery energy storage systems can provide rapid reactive-power support through their converter interfaces. Beyond their conventional energy-management role, BESS converters can be controlled to support the voltage magnitude at the point of common coupling and to influence the interaction between converter controls and the surrounding network [12].

In the present study, the BESS is therefore considered primarily as a dynamic reactive-power and voltage-support resource. The objective is to determine whether inclusion of the BESS $Q(U)$ droop controller modifies the eigenvalue characteristics of the integrated offshore wind–HVDC–grid system under the investigated weak-grid operating condition.

5.2 Integration and Control of Energy Storage

The BESS is connected to the onshore AC network through a voltage-source converter.

Detailed electrochemical, thermal, ageing, and cell-level battery dynamics are not retained because the analysis focuses on the influence of the converter-based voltage-support controller on system-level small-signal behaviour.

The BESS converter operates using reactive-power $Q(U)$ droop control. The reactive-power reference varies in response to deviations in the PCC voltage magnitude. In small-signal form, the controller behaviour is represented by

$$T_q \Delta \dot{q}_{\text{bess}} = -\Delta q_{\text{bess}} - K_{QU} \Delta v_{\text{PCC}}, \qquad (49)$$

where T_q is the BESS reactive-power-control time constant, K_{QU} is the reactive-power droop gain, and Δv_{PCC} is the small-signal deviation in the PCC voltage magnitude.

When the PCC voltage falls below its steady-state value, the controller modifies the BESS reactive-power output in accordance with the adopted droop convention. This response supports the local voltage magnitude and influences the voltage signal measured by the onshore PLL.

The BESS model also contains an SOC state. Under the operating conditions considered, sustained active-power exchange is limited and the SOC evolves on a substantially slower time scale than the converter-control and DC-link states. The SOC state is therefore represented as an integrator in the reduced-order model and is treated separately when evaluating the critical dynamic eigenvalue.

5.3 Comparison of Cases With and Without BESS

The influence of BESS voltage support is assessed by comparing the eigenvalue spectra obtained with and without the BESS subsystem. In the BESS-enabled case, the reduced-order model includes the SOC state, the reactive-power-control state, and the coupling associated with the $Q(U)$ droop controller.

In the comparison case, the BESS states and their associated voltage-support coupling are excluded. The network strength, PLL setting, GFM control parameters, DC-link parameters, and operating point are otherwise maintained at the same values. The comparison therefore evaluates whether inclusion of the BESS changes the PLL-related oscillatory mode under the investigated operating condition.

Figure 5 compares the selected PLL-related complex-conjugate eigenvalue pair with and without BESS support. The horizontal axis represents the real part, σ, in s^{-1}, while the vertical axis represents the imaginary part, ω, in rad/s.

Without the BESS, the representative PLL-related

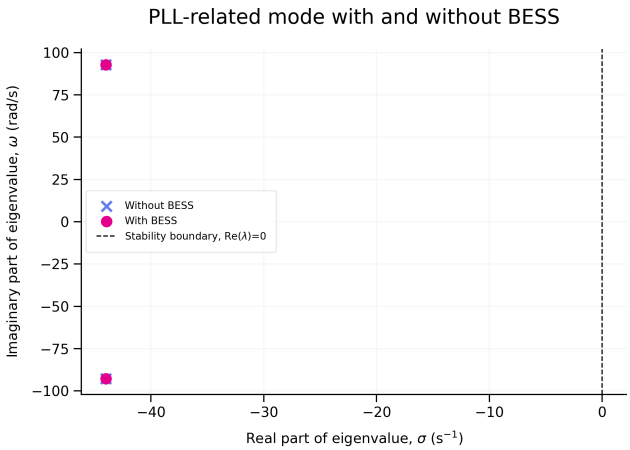


Fig. 5: PLL-related complex-conjugate eigenvalue pair with and without BESS reactive-power $Q(U)$ voltage support. The markers nearly overlap, confirming that BESS inclusion produces no material change in the oscillation frequency or damping ratio under the investigated operating condition. The dashed line denotes the small-signal stability boundary, $\text{Re}(\lambda) = 0$.

Source: Created by the authors.

oscillatory eigenvalue is

$$\lambda_{\text{osc,noBESS}} = -43.9823 + j92.7950. \qquad (50)$$

The corresponding oscillation frequency and damping ratio are 14.7688 Hz and 0.428299, respectively.

With the BESS included, the corresponding eigenvalue is

$$\lambda_{\text{osc,BESS}} = -43.9819 + j92.7955. \qquad (51)$$

The resulting oscillation frequency and damping ratio are 14.7689 Hz and 0.428295, respectively.

The difference between the two oscillatory eigenvalues is very small. At the reported precision, the damping ratio changes by approximately

$$\Delta\zeta_{\text{BESS}} = -4 \times 10^{-6}. \qquad (52)$$

The BESS-enabled case therefore does not demonstrate a material improvement in the damping of the PLL-related oscillatory mode under the investigated operating condition.

The BESS-enabled spectrum additionally contains the expected SOC integrator and reactive-power-control mode. The SOC eigenvalue at the origin represents the slow accumulation of stored energy and is not interpreted as an oscillatory instability. The reactive-power-control mode represents the dynamic response of the BESS converter under $Q(U)$ droop control.

The comparison confirms that the BESS modifies the retained model structure and provides a reactive-power voltage-support function. However, its effect on the principal PLL-related oscillatory mode is negligible compared with the changes observed during the SCR and PLL scaling studies. The result should therefore not be interpreted as evidence of significant damping enhancement or expansion of the stable operating region. Within the adopted eight-state formulation, the principal demonstrated role of the BESS is supplementary PCC-voltage support, while SCR remains the stronger determinant of the damping ratio of the PLL-related mode.

5.4 Interaction Between BESS and PLL Dynamics

The BESS interacts with the PLL-related dynamics through the retained PCC-voltage-support path. Under weak-grid conditions, converter-current perturbations produce comparatively larger PCC-voltage deviations because of the increased equivalent network impedance. These deviations enter the PLL synchronisation loop and contribute to the converter–grid interaction discussed in Section 4.4.

The BESS $Q(U)$ droop controller responds to PCC-voltage deviations by modifying the reactive-power output of the BESS converter. This control action is represented in the reduced-order model by the BESS reactive-power state, Δq_{bess}, and its coupling to the retained PCC-voltage and PLL dynamics.

The resulting voltage-support interaction can be represented qualitatively as

$$\Delta v_{\text{PCC}} \longrightarrow \Delta q_{\text{bess}} \longrightarrow \Delta v_{\text{PCC}}. \tag{53}$$

The first relationship represents the response of the $Q(U)$ droop controller to a PCC-voltage deviation, while the second represents the influence of BESS reactive-power output on the local voltage.

This control function differs from direct active-power or frequency-response control. In the configuration considered, the BESS does not provide fast active-power modulation in response to PLL frequency deviations. Its contribution arises principally from reactive-power and PCC-voltage support.

The numerical comparison in Section 5.3 shows that BESS inclusion produces only a negligible change in the PLL-related oscillatory mode. The damping ratio changes from 0.428299 without BESS to 0.428295 with BESS, corresponding to $\Delta\zeta_{\text{BESS}} \approx -4 \times 10^{-6}$. The oscillation frequency similarly remains approximately constant at 14.77 Hz.

Accordingly, the investigated eight-state model does not demonstrate that BESS inclusion materially improves the damping of the PLL-related mode. The principal effect represented by the BESS states is the addition of reactive-power-control and slow SOC dynamics, together with supplementary PCC-voltage support.

The negligible change in the PLL-related eigenvalue does not imply that BESS voltage support is ineffective in all weak-grid applications. The dynamic influence of a BESS depends on the converter rating, available reactive-power capability, droop gain, controller time constant, network impedance, operating condition, and the strength of the coupling between PCC-voltage and converter-control states.

The original analysis evaluates only cases with and without the BESS subsystem. It does not include a systematic variation of the BESS reactive-power droop gain. The results therefore cannot be used to identify an optimum value of K_{QU} or to establish a general relationship between increasing BESS gain and modal damping. The comparison also does not demonstrate an expansion of the stable operating region. Establishing such an expansion would require a coordinated multi-parameter analysis in which stability boundaries are evaluated over combinations of SCR, PLL bandwidth, and BESS-control settings.

The BESS result is therefore interpreted conservatively. Within the investigated operating condition and retained model structure, the BESS provides a supplementary PCC-voltage-support function but has no material influence on the damping or frequency of the principal PLL-related oscillatory mode.

5.5 Engineering Implications

The results show that the principal small-signal stability drivers in the investigated system are the onshore grid strength and the PLL dynamics. The SCR study produced a clear variation in the damping ratio of the PLL-related oscillatory mode, while the PLL scaling study produced a substantial change in the modal frequency. These effects are considerably greater than the change observed following BESS inclusion.

The BESS should therefore not be regarded as a substitute for appropriate PLL tuning or adequate network strength. Instead, the BESS converter provides a supplementary reactive-power and PCC-voltage-support function through its $Q(U)$ droop controller. This function may remain valuable for voltage regulation even where the calculated influence on the principal oscillatory mode is negligible.

For the investigated operating condition, the

damping ratio of the PLL-related mode changes from 0.428299 without BESS to 0.428295 with BESS. This difference is too small to support a claim of material damping enhancement. The engineering value of the BESS in the present model is therefore associated primarily with its voltage-support capability rather than with direct improvement of the PLL-mode damping.

The limited modal influence also indicates that the effectiveness of BESS support depends on the strength of the coupling between the PCC voltage, BESS reactive-power controller, and converter synchronisation dynamics. This coupling is influenced by the equivalent network impedance, BESS converter rating, available reactive-power capacity, droop gain, controller time constant, and selected operating point.

From a planning perspective, BESS voltage support should be considered as one component of a coordinated converter-control strategy. Grid strength and PLL tuning should first be assessed to determine the principal oscillatory sensitivity. The BESS controller can then be evaluated as a supplementary voltage-regulation measure, subject to converter capability and operating limits.

The results should not be used to determine an optimum value of K_{QU} because the original analysis did not include a systematic BESS droop-gain sweep. Similarly, the comparison does not establish that BESS inclusion expands the stable operating region over a range of SCR and PLL settings.

A more complete engineering assessment would require a coordinated parameter study involving SCR, PLL bandwidth, BESS droop gain, and BESS converter rating. The analysis should also include nonlinear RMS or electromagnetic-transient simulations to evaluate current limits, controller saturation, voltage recovery, fault response, and large-disturbance behaviour.

Within the scope of the present study, the defensible engineering interpretation is that SCR and PLL dynamics determine the principal oscillatory characteristics, while the BESS provides supplementary reactive-power and PCC-voltage support with no material change in the calculated PLL-mode damping.

5.6 Summary

This section evaluated the influence of BESS inclusion by comparing the eigenvalue spectra obtained with and without reactive-power $Q(U)$ voltage support. The adopted BESS representation includes a slow SOC integrator and a reactive-power-control state that responds to PCC-voltage deviations.

The numerical comparison shows that BESS inclusion produces no material change in the principal PLL-related oscillatory mode under the investigated operating condition. The damping ratio changes from 0.428299 without BESS to 0.428295 with BESS, while the oscillation frequency remains approximately 14.77 Hz.

The BESS-enabled model additionally contains the expected SOC integrator and reactive-power-control mode. These states represent the slow energy-storage behaviour and the dynamic response of the converter-based $Q(U)$ droop controller, respectively. The SOC mode is treated separately and is not interpreted as an oscillatory instability.

The principal demonstrated role of the BESS in the retained model is supplementary reactive-power and PCC-voltage support. Its influence on the PLL-related oscillatory mode is negligible compared with the changes associated with SCR and PLL natural-frequency scaling.

Accordingly, the results do not establish significant modal-damping enhancement, an optimum value of K_{QU}, or an expansion of the stable operating region. Establishing such effects would require a systematic BESS droop-gain study, consistent model dimensions across all comparison cases, and additional nonlinear validation.

Within the scope of the present study, SCR remains the principal parameter affecting the damping ratio of the PLL-related mode, while PLL scaling primarily determines its oscillation frequency. The BESS is therefore interpreted as a complementary voltage-support resource rather than as the primary means of improving small-signal damping.

6 Conclusion

This paper investigated the small-signal stability of an offshore wind farm integrated with a weak onshore AC network through a VSC-HVDC transmission system. Particular attention was given to the influence of grid strength, PLL tuning, converter-control dynamics, DC-link behaviour, wind-power loading, and supplementary BESS reactive-power support.

A reduced-order linearised state-space model was used to represent the dominant low-frequency dynamics of the integrated system. The retained states include the offshore GFM frequency and voltage-control states, the onshore PLL angle and frequency states, the filtered active-power state, the DC-link voltage state, the BESS SOC integrator, and the BESS reactive-power-control state.

The model provides a transparent basis for examining eigenvalue locations, damping ratios, oscillation frequencies, state participation, and

sensitivity to selected network and controller parameters. Within the adopted eight-state formulation, the principal complex-conjugate mode is associated predominantly with the onshore PLL synchronisation states.

The SCR sensitivity study showed that decreasing grid strength increases the imaginary component and oscillation frequency of the PLL-related mode, while its real part remains approximately constant at -43.98 s^{-1} over the investigated range. The oscillation frequency increases from 10.05 Hz at SCR $= 10$ to 23.54 Hz at SCR $= 1$.

Because the imaginary component increases relative to the nearly constant real part, the damping ratio decreases from 0.571 at SCR $= 10$ to 0.285 at SCR $= 1$. These results demonstrate that weaker-grid conditions reduce the relative damping of the PLL-related oscillatory mode within the retained model.

The PLL sensitivity study showed that increasing the PLL natural-frequency scaling factor substantially increases the oscillation frequency of the PLL-related mode. The frequency increases from 7.41 Hz at $k_{\text{PLL}} = 0.5$ to 29.51 Hz at $k_{\text{PLL}} = 2.0$.

The real and imaginary components of the PLL-related eigenvalue pair increase in approximately the same proportion during the PLL scaling study. The damping ratio consequently remains nearly constant at approximately 0.428. The retained eight-state model therefore demonstrates strong modal-frequency sensitivity to PLL tuning, but it does not demonstrate progressive damping degradation as the PLL scaling factor increases.

The SCR and PLL studies consequently reveal two distinct sensitivities of the same PLL-related oscillatory mode. Grid strength primarily affects the mode's relative damping characteristics, whereas the PLL natural-frequency scaling factor primarily determines its oscillation frequency. These results show that network strength and PLL tuning should be assessed together during converter-control design.

Within the retained formulation, the offshore GFM frequency and voltage dynamics are represented by first-order states. The influence of GFM droop and virtual inertia is therefore interpreted through changes in the decay characteristics of the corresponding real modes rather than through a separate GFM oscillatory eigenvalue pair.

The active-power-control and DC-link voltage states similarly contribute primarily to non-oscillatory modes over the investigated parameter range. The wind-loading study produces comparatively small changes in the retained eigenvalue characteristics, indicating that the model is more sensitive to grid strength and converter-control settings than to changes in wind-power loading.

The BESS was represented as a converter-interfaced reactive-power resource operating under $Q(U)$ droop control. Its principal function in the model is supplementary PCC-voltage support. The representative PLL-related eigenvalue changes from $-43.9823 + j92.7950$ without BESS to $-43.9819 + j92.7955$ with BESS.

The corresponding damping ratio changes from 0.428299 without BESS to 0.428295 with BESS, while the oscillation frequency remains approximately 14.77 Hz. This difference is negligible and does not demonstrate material damping enhancement of the principal PLL-related mode under the investigated operating condition.

The BESS-enabled model additionally contains the expected SOC integrator and reactive-power-control mode. These states represent the slow energy-storage behaviour and the dynamic response of the converter-based voltage-support controller. The SOC integrator is treated separately and is not interpreted as an oscillatory instability.

The results therefore do not establish significant BESS damping enhancement, an optimum value of K_{QU}, or an expansion of the stable operating region. The BESS is instead interpreted as a complementary voltage-support resource whose modal influence depends on its converter rating, available reactive-power capability, controller parameters, network impedance, and operating condition.

The principal contribution of this work is the integrated interpretation of grid strength, PLL dynamics, DC-link behaviour, GFM control characteristics, wind-power loading, and BESS voltage support within a transparent reduced-order framework. The analysis identifies the PLL synchronisation subsystem as the principal source of oscillatory behaviour in the retained model.

The discrete parameter studies are not intended to establish a universal critical SCR, maximum allowable PLL bandwidth, or closed-form stability boundary. Such quantities depend on the complete converter-control structure, network impedance, component ratings, operating point, and model assumptions.

Future work should include nonlinear RMS and electromagnetic-transient validation of the identified modal trends. Further investigation should consider systematic variation of the BESS $Q(U)$ droop gain, consistent model dimensions for BESS comparisons, converter-current limiting, controller saturation, large-disturbance behaviour, grid-forming control extensions, and multi-terminal HVDC configurations [14].

Acknowledgment:
The authors would like to thank the University of KwaZulu-Natal and Eskom Holdings SOC Limited for the support provided during this research. The authors also acknowledge the technical guidance and discussions that contributed to the development of the study.

References:

[1] Dirk Van Hertem, Oriol Gomis-Bellmunt, and Jun Liang, editors. *HVDC Grids: For Offshore and Supergrid of the Future*. Wiley-IEEE Press, Hoboken, NJ, USA, 2016. ISBN: 978-1-118-85915-5. https://doi.org/10.1002/9781119115243.

[2] István Erlich, Fekadu Shewarega, Christian Feltes, Friedrich W. Koch, and Jens Fortmann. Offshore wind power generation technologies. *Proceedings of the IEEE*, 101(4):891–905, 2013. https://doi.org/10.1109/JPROC.2012.2225591.

[3] Prabha Kundur. *Power System Stability and Control*. McGraw-Hill, New York, NY, USA, 1994. ISBN: 978-0-07-035958-1. https://www.abebooks.com/9780070359581/Power-System-Stability-Control-Kundur-007035958X/plp, accessed 13 October 2026.

[4] Jan Machowski, Janusz W. Bialek, and James R. Bumby. *Power System Dynamics: Stability and Control*. John Wiley & Sons, Chichester, U.K., 2nd edition, 2008. ISBN: 978-0-470-72558-0. https://books.google.com/books?id=wZv92UdKxi4C, accessed 13 October 2026.

[5] M. J. Gibbard, P. Pourbeik, and D. J. Vowles. *Small-Signal Stability, Control and Dynamic Performance of Power Systems*. University of Adelaide Press, Adelaide, Australia, 2015. ISBN: 978-1-925261-03-5. https://doi.org/10.20851/small-signal.

[6] Federico Milano, Florian Dörfler, Gabriela Hug, David J. Hill, and Gregor Verbič. Foundations and challenges of low-inertia systems. In *Proceedings of the 2018 Power Systems Computation Conference (PSCC)*, pages 1–25, Dublin, Ireland, 2018. IEEE. https://doi.org/10.23919/PSCC.2018.8450880.

[7] Nikos Hatziargyriou, Jovica Milanović, Claudia Rahmann, Venkataramana Ajjarapu, Claudio A. Cañizares, István Erlich, David J. Hill, Ian A. Hiskens, Innocent Kamwa, Bikash Pal, Pouyan Pourbeik, Juan J. Sanchez-Gasca, Aleksandar Stanković, Thierry Van Cutsem, Vijay Vittal, and Costas D. Vournas. Definition and classification of power system stability revisited and extended. *IEEE Transactions on Power Systems*, 36(4):3271–3281, 2021. https://doi.org/10.1109/TPWRS.2020.3041774.

[8] Jian Sun. Impedance-based stability criterion for grid-connected inverters. *IEEE Transactions on Power Electronics*, 26(11):3075–3078, 2011. https://doi.org/10.1109/TPEL.2011.2136439.

[9] Bo Wen, Dushan Boroyevich, Rolando Burgos, Paolo Mattavelli, and Zhiyu Shen. Analysis of d-q small-signal impedance of grid-tied inverters. *IEEE Transactions on Power Electronics*, 31(1):675–687, 2016. https://doi.org/10.1109/TPEL.2015.2398192.

[10] Claudio Burgos-Mellado, Alessandro Costabeber, Mark Sumner, Roberto Cárdenas-Dobson, and Doris Sáez. Small-signal modelling and stability assessment of phase-locked loops in weak grids. *Energies*, 12(7):1227, 2019. https://doi.org/10.3390/en12071227.

[11] Dinesh Pattabiraman, Robert H. Lasseter, and Thomas M. Jahns. Impact of phase-locked loop control on the stability of a high inverter penetration power system. In *Proceedings of the 2019 IEEE Power & Energy Society General Meeting (PESGM)*, pages 1–5. IEEE, 2019. https://doi.org/10.1109/PESGM40551.2019.8973657.

[12] Francisco Díaz-González, Andreas Sumper, Oriol Gomis-Bellmunt, and Roberto Villafáfila-Robles. A review of energy storage technologies for wind power applications. *Renewable and Sustainable Energy Reviews*, 16(4):2154–2171, 2012. https://doi.org/10.1016/j.rser.2012.01.029.

[13] Lujie Yu, Rui Li, and Lie Xu. Distributed pll-based control of offshore wind turbines connected with diode-rectifier-based hvdc systems. *IEEE Transactions on Power Delivery*, 33(3):1328–1336, 2018. https://doi.org/10.1109/TPWRD.2017.2772342.

[14] Robert H. Lasseter, Zhe Chen, and Dinesh Pattabiraman. Grid-forming inverters: A critical asset for the power grid. *IEEE Journal of Emerging and Selected Topics in Power Electronics*, 8(2):925–935, 2020. https://doi.org/10.1109/JESTPE.2019.2959271.

Contribution of Individual Authors to the Creation of a Scientific Article:

Andile S. Xaba contributed to the conceptualization, methodology, software development, formal analysis, investigation, data curation, visualization, and preparation and revision of the manuscript. Rudiren Sarma contributed to the supervision of the underlying research and provided technical and methodological guidance. David G. Dorrell contributed to the supervision of the underlying research and provided technical guidance. The corresponding author prepared the present revised version in response to the reviewers' comments.

Sources of Funding for Research Presented in the Scientific Article:

No specific external research grant was received for conducting this study. Institutional and publication-related support was provided by the University of KwaZulu-Natal and Eskom Holdings SOC Limited.

Conflicts of Interest:

The authors declare that there are no conflicts of interest relevant to the content of this article.

Creative Commons Attribution License 4.0 (Attribution 4.0 International , CC BY 4.0)

This article is published under the terms of the Creative Commons Attribution License 4.0
https://creativecommons.org/licenses/by/4.0/deed.en_US